Progress In Electromagnetics Research, Vol. 156, 55–62, 2016

Negative Group Delay Phenomenon Analysis Using Finite Unloaded Quality Factor Resonators

Girdhari Chaudhary and Yongchae Jeong*

Abstract—This paper presents a comprehensive method to analyze negative group delay (NGD) phenomenon at microwave frequency. This method is based on a coupling matrix with finite unloaded quality factor resonators. Unlike conventional NGD circuit topologies that use a lumped resistor R along with bandstop resonators, the proposed topology does not require any R for generating NGD and therefore, provides fully distributed circuit realization. The proposed topology has both source to load and inter-resonator coupling structures. Analytical design equations are provided to obtain predefined NGD with matched input/output ports; the proposed structure therefore does not require any extra matching networks. From analytical analysis, it is also found that the NGD bandwidth as well as magnitude flatness can be controlled by inter-resonator couplings. The proposed design theory is proven through fabrications of NGD circuit at a center frequency of 2.14 GHz. The measurement results are in good agreement with simulations and predicted theoretical results.

1. INTRODUCTION

Frequency-dependent group delay (GD) is inversely proportional to group velocity and can be examined by the phase (φ) variation of a forward transmitting scattering parameter. Mathematically, the GD is defined by the differential-phase relation as in Eq. (1).

$$\tau_g = -\frac{d\varphi}{d\omega}. \tag{1}$$

Using Eq. (1), the presence of negative group delay (NGD) in medium is equivalent to increasing a phase (positive slope) with a frequency. Therefore, the NGD refers to the phenomenon whereby an electromagnetic wave traverses a dispersive material or electronic circuit in such a manner that its amplitude envelope is advanced through media rather than undergoing delay [1–3]. However, this phenomenon does not violate a causality, since the initial transient of the pulse is still limited to the front velocity that does not exceed the speed of light in a vacuum [2, 3]. The effect of NGD is observed within a limited frequency band when the absorption or attenuation is at a maximum. Therefore, conventional approaches to realize the NGD circuits are based on bandstop structures using either series or shunt RLC resonators [4–11]. The NGD circuits have been used in various practical applications in communication systems, such as shortening or reducing delay lines [11], enhancing the efficiency of feedforward linear amplifiers [12, 13], designing broadband and constant phase shifters [14], realization of non-Foster reactive elements [15], and minimizing beam-squint in series-fed antenna arrays [16].

To overcome the limited availability problem of lumped elements in a microwave regime, the NGD circuits have been designed using distributed transmission line resonators along with the resistor (R) because NGD cannot be exhibited without R [17–22]. Moreover, the conventional NGD circuits suffer

Received 11 April 2016, Accepted 11 June 2016, Scheduled 17 June 2016

* Corresponding author: Yongchae Jeong (ycjeong@jbnu.ac.kr).

The authors are with the Division of Electronics and Information Engineering, IT Convergence Research Center, Chonbuk National University, 567 Baekjae Daero, Deokjin-gu, Jeonju-si, Jeollabuk-do 54896, Republic of Korea.

from several disadvantages such as high signal attenuation (SA), small NGD bandwidth and magnitude (S_{21}) flatness. While a few works have been done for reducing SA [19–22], these works still suffer from small NGD bandwidth and magnitude flatness problem. To overcome these problems, researchers have attempted to design NGD circuits using different methods such as cross-coupling between resonators [23], increasing the number of resonators [24] and transversal-filter topologies [25]. On the other hand, these works showed very high SA ($>$ 28 dB for -1 ns). Moreover, except for the work of [25], these NGD circuits also used R for generating NGD, which prevents fully distributed circuit realization.

The coupling matrix method is widely used to design narrow band filters with different functionalities such as tunable center frequency (f_0) and bandwidth, switchable filter from bandstop to all-pass filter, and bandstop to bandpass switchable filter [26–28].

This paper presents the design of a fully distributed NGD circuit with predefined NGD, good magnitude flatness, and wide NGD bandwidth. The design method is based on a coupling matrix along with finite unloaded-quality factor (Q_u) resonators. This proposed topology does not require any R for generating NGD, or any extra network for matching input/output ports with reference termination impedances. Therefore, the proposed work allows fully distributed transmission line circuit realization.

2. DESIGN METHOD

Figure 1 shows a coupling diagram of the proposed NGD topology where input/output external couplings (M_{S1} and M_{L2}) are equal. Similarly, the resonator self-coupling values (M_{11} and M_{22}), source-to-load (M_{SL}) coupling, and load-to-source coupling (M_{LS}) have the same magnitude.

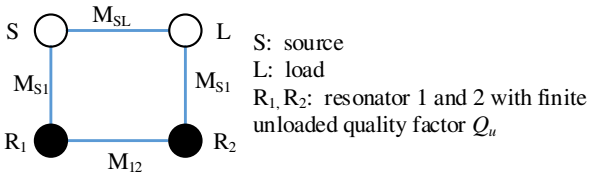

Figure 1. Coupling diagram of the proposed NGD topology.

$(N+2)\times(N+2)$ coupling matrix of the proposed topology corresponding to the coupling diagram shown in Fig. 1 is given as Eq. (2).

$$M = \begin{bmatrix} 0 & M_{S1} & 0 & M_{SL} \\ M_{S1} & M_{11} & M_{12} & 0 \\ 0 & M_{12} & M_{22} & M_{S1} \\ M_{SL} & 0 & M_{S1} & 0 \end{bmatrix} \tag{2}$$

where subscripts S, L, 1, and 2 correspond to the source, load, first resonator and second resonator, respectively.

Assuming that the coupling between source and load (M_{SL}) is lossless, the reflection (S_{11}) and transmission (S_{21}) responses corresponding to the coupling relationship (2) are given in Eq. (3) with finite Q_u resonators. In this equation, Ω is the normalized frequency in rad/s, and Δ is a 3-dB fractional bandwidth [26, 28].

$$S_{11} = 1 - \left\{ \frac{2\left(\begin{array}{l} \Omega^4 - M_{S1}^2\Omega^2\left(M_{S1}^2 + 2j\Omega\right) - M_{12}^2\left(2\Omega^2 - M_{12}^2 - 2jM_{S1}^2\Omega\right) + \frac{1}{Q_u^4\Delta^4} \\ + \frac{2\left(M_{S1}^2+2j\Omega\right)}{Q_u^3\Delta^3} + \frac{2M_{12}^2+M_{S1}^2\left(M_{S1}^2+6j\Omega\right)-6\Omega^2}{Q_u^2\Delta^2} + \frac{2M_{S1}^2\left(M_{12}^2-3\Omega^2+jM_{S1}^2\Omega\right)+4j\Omega\left(M_{12}^2-\Omega^2\right)}{Q_u\Delta} \end{array} \right)}{\left(\Omega^2 - M_{12}^2 - \frac{1}{Q_u^2\Delta^2} - \frac{\left(M_{S1}^2+2j\Omega\right)}{Q_u\Delta} - jM_{S1}^2\Omega\right)\left\{ \begin{array}{l} \left(1+M_{SL}^2\right)\left(\Omega^2 - M_{12}^2 - \frac{1}{Q_u^2\Delta^2}\right) \\ -\frac{2}{Q_u\Delta}\left(M_{S1}^2 + jM_{SL}^2\Omega + j\Omega\right) \\ +M_{S1}^2\left(2M_{SL}M_{12} - M_{s1}^2 - 2j\Omega\right) \end{array} \right\}} \right\} \tag{3a}$$

$$S_{21} = \frac{\frac{2M_{SL}}{Q_u\Delta}\Omega + j\left(M_{SL}\Omega^2 + M_{S1}^2M_{12} - M_{SL}M_{12}^2 - \frac{M_{SL}}{Q_u^2\Delta^2}\right)}{\left\{\frac{M_{S1}^4}{2} + \frac{\left(M_{SL}^2+1\right)M_{12}^2}{2} - \frac{\left(M_{SL}^2+1\right)}{2}\Omega^2 + \frac{M_{S1}^2}{Q_u\Delta} + \frac{\left(M_{SL}^2+1\right)}{2Q_u^2\Delta^2} - M_{S1}^2M_{12}M_{SL} + j\left(M_{S1}^2 + \frac{M_{SL}^2+1}{Q_u\Delta}\right)\Omega\right\}} \tag{3b}$$

For matched input/output ports, S_{11} in Eq. (3a) is set to zero at $\Omega = 0$ in order to solve the relation between M_{SL} and M_{S1} with the assumption of $M_{12} = aM_{S1}^2$, where a is any real positive value. For any arbitrary value of M_{S1}, the relation between M_{SL} and M_{S1} for matched input/output ports at $\Omega = 0$ can be found as Eq. (4).

$$M_{SL} = \frac{aM_{S1}^4 - \sqrt{a^2M_{S1}^8 - b\left(a^2M_{S1}^4 + \frac{1}{Q_u^2\Delta^2}\right)}}{\left(a^2M_{S1}^4 + \frac{1}{Q_u^2\Delta^2}\right)} \tag{4}$$

where

$$b = \left(M_{S1}^4 + a^2M_{S1}^4 + \frac{1}{Q_u^2\Delta^2} + \frac{2M_{S1}^2}{Q_u\Delta} - \frac{2b_1}{b_2}\right) \tag{5a}$$

$$b_1 = a^4M_{S1}^8 + \frac{1}{Q_u^4\Delta^4} + \frac{2M_{S1}^2}{Q_u^3\Delta^3} + \frac{\left(2a^2+1\right)M_{S1}^4}{Q_u^2\Delta^2} + \frac{2a^2M_{S1}^6}{Q_u\Delta} \tag{5b}$$

$$b_2 = a^2M_{S1}^4 + \frac{1}{Q_u^2\Delta^2} + \frac{M_{S1}^2}{Q_u\Delta} \tag{5c}$$

Furthermore, using Eq. (3b), the GD and magnitude of the proposed topology at $\Omega = 0$ can be calculated as Eq. (6), where M_{SL} can be obtained from Eq. (4) for the matched input/output condition.

$$|S_{21}|_{\Omega=0} = \frac{aM_{S1}^4 - a^2M_{SL}M_{S1}^4 - \frac{M_{SL}}{Q_u^2\Delta^2}}{\frac{M_{S1}^4}{2} + \frac{M_{S1}^2}{Q_u\Delta} - aM_{S1}^4M_{SL} + \frac{\left(1+M_{SL}^2\right)\left(1+a^2M_{S1}^4Q_u^2\Delta^2\right)}{2Q_u^2\Delta^2}} \tag{6a}$$

$$\tau_g|_{\Omega=0} = \frac{\frac{2M_{SL}}{Q_u\Delta}}{aM_{S1}^4 - a^2M_{SL}M_{S1}^4 - \frac{M_{SL}}{Q_u^2\Delta^2}} + \frac{M_{S1}^2 + \frac{M_{SL}^2+1}{Q_u\Delta}}{\frac{M_{S1}^4}{2} + \frac{\left(1+M_{SL}^2\right)\left(1+a^2M_{S1}^4Q_u^2\Delta^2\right)}{2Q_u^2\Delta^2} + \frac{M_{S1}^2}{Q_u\Delta} - aM_{S1}^4M_{SL}} \tag{6b}$$

To illustrate the above design equations, the calculated responses of the proposed topology are shown in Fig. 2 for different values of the coupling matrix. The calculated coupling matrix for $S_{11} = 0$ at $\Omega = 0$ is shown in Table 1. As observed from Fig. 2(a), the input/output output ports are matched at $\Omega = 0$ and higher than -10 dB for $-2 < \Omega < 2$. Similarly, S_{21} is decreased as M_{12} increases toward a higher value. Moreover, the maximum GD at $\Omega = 0$ and the NGD bandwidth (which is defined as bandwidth when GD < 0) are also increased when M_{12} is changed from 0.2738 to 0.5476 as shown in Fig. 2(b) implying the need for controlling the coupling between resonators 1 and 2. Therefore, a strong

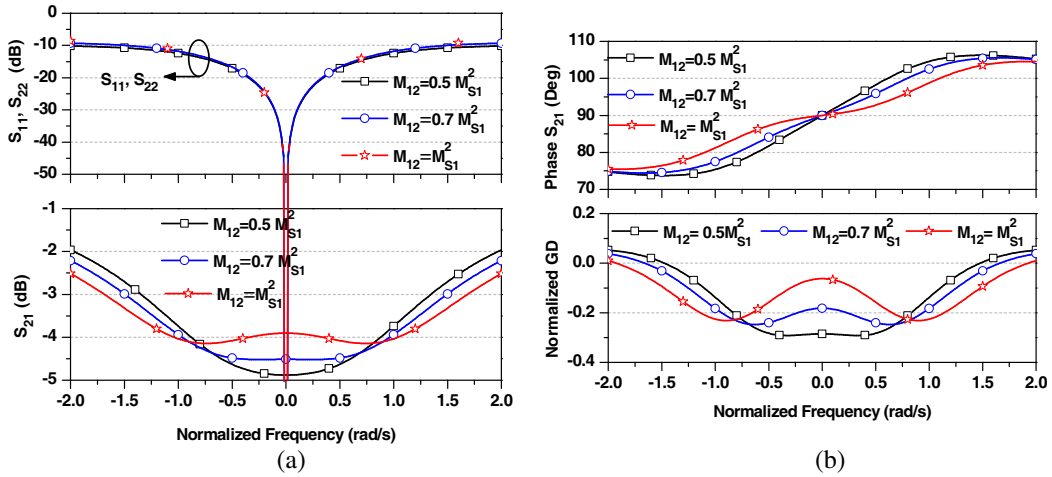

Figure 2. Calculated response of the proposed NGD topology with $M_{S1} = 0.74$, $Q_u = 50$, $\Delta = 2\%$: (a) S-parameter magnitudes and (b) phase/group delay characteristics.

Table 1. Coupling matrix, group delay and S-parameters at normalized center frequency.

$M_{S1}=0.74$, $Q_u=50$, $\Delta=2\%$, $\lvert S_{11}\rvert_{\Omega=0}=0$					
a	M_{12}	M_{SL}	$\lvert S_{11}\rvert_{\Omega=0}$ (dB)	$\tau_g\rvert_{\Omega=0}$	$\angle S_{21}\rvert_{\Omega=0}$
1	0.5476	−0.6762	−3.9021	−0.0620	90°
0.7	0.3833	−0.6956	−4.5138	−0.1817	90°
0.5	0.2738	−0.7210	−4.8809	−0.2847	90°

coupling is required for a wider NGD bandwidth. However, this decreases the maximum NGD at $\Omega=0$. Therefore, a trade-off occurs among the insertion loss, maximum NGD at $\Omega=0$, and NGD bandwidth.

To demonstrate the effect of Q_u on frequency response and GD, the calculated responses are shown in Fig. 3. For this simulation, values of M_{S1}, M_{12}, and Δ are fixed, whereas Q_u is changed by ±10% from the original value. M_{SL} can be calculated using Eq. (4) for $S_{11}=0$ at $\Omega=0$. The coupling matrix, calculated GD and S-parameter magnitudes at $\Omega=0$ are presented in Table 2. As seen from these results, S_{21} is varied around 0.74 dB for $Q_u\pm10\%$ variation. However, the maximum GD and NGD bandwidth are almost the same.

Similarly, to illustrate the effect of M_{SL} on the frequency response and GD, the calculated responses are shown in Fig. 4. For this simulation, the values of M_{S1}, M_{12}, Q_u, and Δ are fixed whereas M_{SL} is changed by ±10% from the original calculated value using Eq. (4). The coupling matrix, calculated GD and S-parameter magnitudes at $\Omega=0$ are presented in Table 3. When M_{SL} is changed by ±10% variation from the original, the return loss at $\Omega=0$ is slightly degraded. However, it is higher than 27 dB. Moreover, an S_{21} variation around 0.66 dB was also observed. However, this only has a slight variation on the maximum NGD and bandwidth. From Table 3, it is concluded that for the same return

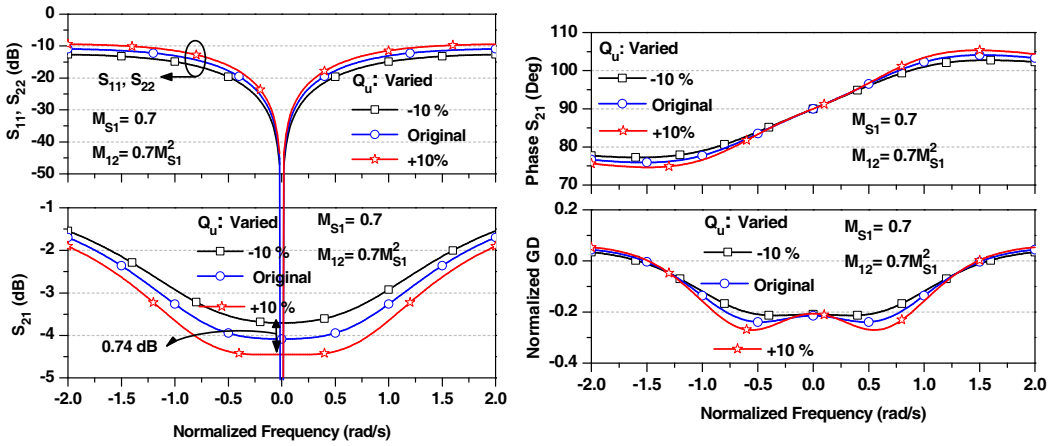

Figure 3. Calculated frequency response with $M_{S1}=0.7$, $Q_u=50$, $\Delta=2\%$, and variation of Q_u: (a) S-parameter magnitudes and (b) phase/group delay characteristics.

Table 2. Coupling matrix, group delay, and S-parameters at normalized center frequency for $Q_u\pm10\%$ variation.

$M_{S1}=0.7$, $M_{12}=0.7M_{S1}^2$, $Q_u=50$, $\Delta=2\%$, $\lvert S_{11}\rvert_{\Omega=0}=0$					
$Q_u\pm10\%$		M_{SL}	$\lvert S_{11}\rvert_{\Omega=0}$ (dB)	$\tau_g\rvert_{\Omega=0}$	$\angle S_{21}\rvert_{\Omega=0}$
−10%	45	−0.7911	−3.7070	−0.2095	90°
Q_u	50	−0.7484	−4.0847	−0.2149	90°
+10%	55	−0.7037	−4.4509	−0.2062	90°

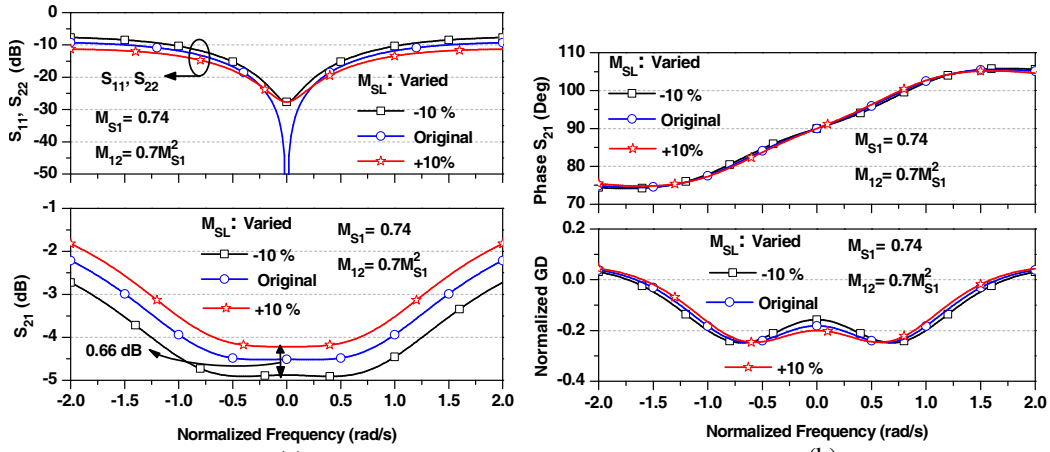

Figure 4. Calculated frequency response with variation of M_{SL} and $M_{S1} = 0.74$, $Q_u = 50$, $\Delta = 2\%$: (a) S-parameter magnitudes and (b) phase/group delay characteristics.

Table 3. Coupling matrix, group delay, and S-parameters at normalized center frequency for $M_{SL}\pm10\%$ variation.

$M_{S1} = 0.74$, $M_{12} = 0.7M_{S1}^2$, $Q_u = 50$, $\Delta = 2\%$					
$M_{SL} \pm 10\%$		$\lvert S_{11}\rvert_{\Omega=0}$ (dB)	$\lvert S_{21}\rvert_{\Omega=0}$ (dB)	$\tau_g\rvert_{\Omega=0}$	$\angle S_{21}\rvert_{\Omega=0}$
-10%	-0.6260	-27.6546	-4.8785	-0.1573	$90°$
M_{SL}	-0.6956	$-\infty$	-4.5138	-0.1817	$90°$
$+10\%$	-0.7652	-27.6959	-4.2178	-0.2003	$90°$

loss value, a higher M_{SL} is preferable because S_{21} is less, and maximum NGD at $\Omega = 0$ is higher than the original in this case.

3. SIMULATION AND MEASUREMENT

For experimental demonstration purposes, the proposed NGD topology was fabricated at f_0 of 2.14 GHz on an FR-4 epoxy substrate with a dielectric constant (ε_r) of 4.4, thickness (h) of 0.787 mm, and loss tangent of 0.02. The physical dimensions of the fabricated circuits were optimized using ANSYS HFSS 15.

The design goal was to achieve a maximum GD of -1 ns and insertion loss of 3.8 dB at f_0 2.14 GHz under the assumption of termination port impedance Z_0 of 50 Ω. As described for the design equations of the proposed topology in the previous section, the coupling matrix is extracted for the given specification as $M_{S1} = 0.69$, $M_{12} = 0.3468$, $M_{SL} = -0.7677$ with $Q_u = 50$ and $\Delta = 2\%$.

The resonators are implemented with an open-circuited $\lambda/2$ transmission line. Using HFSS Eigen-mode simulation, Q_u of the $\lambda/2$ resonator in the FR-4 epoxy substrate is estimated to be around 50. Similarly, the coupling between the source and load is implemented with a step-impedance $3\lambda/4$ line. The EM layout and photograph of the fabricated circuit are shown in Fig. 5. The physical dimensions after EM simulation optimization are presented in Table 4. The coupling coefficients between

Table 4. Physical dimension of fabricated circuit (refer to Fig. 5). Units: mm.

L_0	L_1	L_2	L_3	L_4	L_5	W_1	W_2	W_3	g_1	g_2
6.8	12.3	17.4	14.1	1.5	19.9	1.8	3.8	1.8	0.6	6

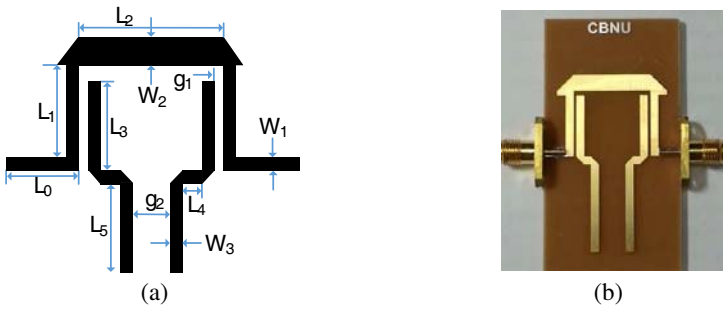

(a) (b)

Figure 5. (a) EM simulation layout with physical dimensions and (b) photograph of fabricated circuit.

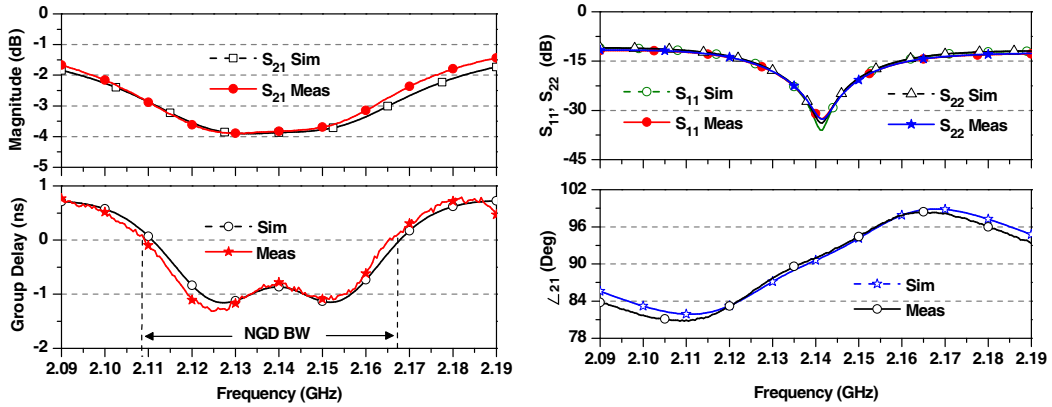

(a) (b)

Figure 6. Simulation and measured results of the proposed negative group delay circuit: (a) magnitude/group delay and (b) return loss/phase characteristics.

Table 5. Performance comparison of proposed NGD circuit with other works.

	f_0 (GHz)	$\mathrm{GD}_{\max}$ (ns)	$S_{21\,\max}$ (dB)	R
[4, 5]	1.0	−10	−30	Yes
[6]*	1.0	−2	2	Yes
[9, 10]*	0.31	−1.52	0.290	Yes
[11]	0.55	−6	x	Yes
[12, 13]	2.14	−9	−64.2	Yes
[17, 18]	2.14	−5.65	−62.6	Yes
[19]	2.14	−6.40	−14.3	Yes
[20]	2.14	−7.9	−16.5	Yes
[21]	2.14	−7.48	−17.45	Yes
[22]	2.14	−6.85	−15.38	Yes
[23]**	1.962	−1.10	−29.3	Yes
[24]	1.962	−6.50	−21.2	Yes
[25]	1.0	−1.50	−37	No
This work	**2.14**	−1.03	−3.82	**No**

$*$ = Gain compensated active NGD circuits

R = Does resistor R required to generated NGD?

$**$ = Return loss (S_{11}) < 1 dB which needs extra matching network

source/load and resonators R_1/R_2 are controlled by varying L_3 and g_1. Similarly, the inter-resonator coupling coefficient is controlled by changing L_5 and g_2.

The simulated and measured results are shown in Fig. 6. The measurement results are in good agreement with the simulations. From the measurement results, the insertion loss and GD of S_{21} at $f_0 = 2.14\,\text{GHz}$ are determined as 3.82 dB and $-1.031 \pm 0.24\,\text{ns}$, respectively. The NGD bandwidth is determined as 60 MHz, providing the NGD-bandwidth product of 0.062. Similarly, the measured return loss and phase at f_0 are obtained as 30.48 dB and 90.96°, respectively. Moreover, the return loss is higher than 12 dB in the frequency range of 100 MHz.

Table 5 shows a comparison of the performance of the proposed NGD circuit with the previous works. Considering the low SA, NGD, and magnitude flatness bandwidth, the proposed structure provides a better performance than previous works. Another advantage of the proposed work is that it does not require any additional R to generate NGD, which provides a fully distributed transmission line implementation of the circuit.

4. CONCLUSION

In this paper, we investigate a comprehensive method to design a negative group delay circuit with low signal attenuation, wide NGD bandwidth and good magnitude flatness based on a coupling matrix along with a resonator's finite unloaded-quality factor. Analytical design equations are provided to obtain the predefined negative group delay. The proposed method provides a simple way to create wider NGD bandwidths with a flatness response. The design theory is validated by fabricating microstrip negative group delay circuit at a center frequency of 2.14 GHz. The measurement results show good agreement with the simulations as well as the theoretical predicted values. Another advantage of the proposed circuit topology is that circuits do not need any additional lumped elements and therefore is very suitable for high frequency, in which lumped elements are not obtainable. The proposed circuit can be applied in various applications such as the realization of a non-Foster reactive element and series-fed antenna arrays for minimizing beam-squint problem. Future research may include development of the negative group delay topology for odd number of filter stages.

ACKNOWLEDGMENT

This research was supported by the Basic Science Research Program through the National Research Foundation of Korea (NRF) funded by the Ministry of Education, Science, and Technology (2013006660).

REFERENCES

1. Hymel, C. H., M. H. Skolnick, R. A. Stubbers, and M. E. Brandt, "Temporally advanced signal detection: A review of technology and potential applications," *IEEE Circuit and Systems Magazine*, Vol. 11, No. 3, 10–25, Aug. 2011.
2. Brillouin, L. and A. Sommerfeld, *Wave Propagation and Group Velocity*, 113–137, Academic Press Network, New York, 1960.
3. Kandic, M. and G. E. Bridges, "Limits of negative group delay phenomenon in linear causal media," *Progress In Electromagnetics Research*, Vol. 134, 227–246, 2013.
4. Lucyszyn, S., I. D. Robertson, and A. H. Aghvami, "Negative group delay synthesizer," *Electronics Letters*, Vol. 29, No. 9, 798–800, Apr. 1993.
5. Lucyszyn, S. and I. D. Robertson, "Analog reflection topology building blocks for adaptive microwave signal processing applications," *IEEE Trans. Microw. Theory Tech.*, Vol. 43, No. 3, 601–611, Mar. 1995.
6. Ravelo, B., A. Perennec, M. L. Roy, and Y. G. Boucher, "Active microwave circuit with negative group delay," *IEEE Microw. Wireless Compon. Letters*, Vol. 17, No. 12, 861–863, Dec. 2007.
7. Broomfield, C. D. and J. K. A. Everard, "Broadband negative group delay networks for compensation of microwave oscillators and filters," *Electronics Letters*, Vol. 9, No. 23, 1931–1932, Nov. 2000.

8. Choi, H., K. Song, C. D. Kim, and Y. Jeong, "Synthesis of negative group delay time circuit," *Proceedings of Asia Pacific Microwave Conference*, 1–4, 2008.
9. Kandic, M. and G. E. Bridges, "Bilateral Gain-compensated negative group delay circuit," *IEEE Microw. Wireless Compon. Letters*, Vol. 21, No. 6, 308–310, Jun. 2011.
10. Kandic, M. and G. E. Bridges, "Asymptotic limit of negative group delay in active resonator-based distributed circuits," *IEEE Trans. Circuit System-I*, Vol. 58, No. 8, 1727–1735, Aug. 2011.
11. Noto, H., K. Yamauchi, M. Nakayama, and Y. Isota, "Negative group delay circuit for feed-forward amplifier," *Proc. of IEEE Inter. Microw. Symp. Dig.*, 1103–1106, Jun. 2007.
12. Choi, H., Y. Jeong, C. D. Kim, and J. S. Kenney, "Efficiency enhancement of feedforward amplifiers by employing a negative group delay circuit," *IEEE Trans. Microw. Theory Tech.*, Vol. 58, No. 5, 1116–1125, May 2010.
13. Choi, H., Y. Jeong, C. D. Kim, and J. S. Kenney, "Bandwidth enhancement of an analog feedback amplifier by employing a negative group delay circuit," *Progress In Electromagnetics Research*, Vol. 105, 253–272, 2010.
14. Ravelo, B., M. L. Roy, and A. Perennec, "Application of negative group delay active circuits to the design of broadband and constant phase shifters," *Microw. Optical Tech. Letters*, Vol. 50, No. 12, 3078–3080, Dec. 2008.
15. Mirzaei, H. and G. V. Eleftheriades, "Realizing non-Foster reactive elements using negative group delay networks," *IEEE Trans. Microw. Theory Tech.*, Vol. 61, No. 12, 4322–4332, Dec. 2013.
16. Mirzaei, H. and G. V. Eleftheriades, "Arbitrary-angle squint free beamforming in series-fed antenna arrays using non-Foster elements synthesized by negative group delay networks," *IEEE Trans. Antennas and Propagation*, Vol. 63, No. 5, 1997–2010, May 2015.
17. Jeong, Y., H. Choi, and C. D. Kim, "Experimental verification for time advancement of negative group delay in RF electronics circuits," *Electronics Letters*, Vol. 46, No. 4, 306–307, Feb. 2010.
18. Choi, H., Y. Kim, Y. Jeong, and C. D. Kim, "Synthesis of reflection type negative group delay circuit using transmission line resonator," *Proceeding of 39th European Microw. Conf.*, 902–605, Sep. 2009.
19. Choi, H., G. Chaudhary, T. Moon, Y. Jeong, J. Lim, and C. D. Kim, "A design of composite negative group delay circuit with lower signal attenuation for performance improvement of power amplifier linearization techniques," *IEEE Inter. Microw. Symp. Dig.*, 1–4, Jun. 2011.
20. Chaudhary, G. and Y. Jeong, "Distributed transmission line negative group delay circuit with improved signal attenuation," *IEEE Microw. Wireless Compon. Letters*, Vol. 24, No. 1, 20–22, Jan. 2014.
21. Chaudhary, G. and Y. Jeong, "Transmission line negative group delay networks with improved signal attenuation," *IEEE Antenna and Wireless Propag. Letters*, Vol. 13, 1039–1042, 2014.
22. Chaudhary, G. and Y. Jeong, "Low signal attenuation negative group delay network topologies using coupled lines," *IEEE Trans. Microw. Theory Tech.*, Vol. 62, No. 10, 2316–2324, Oct. 2014.
23. Chaudhary, G. and Y. Jeong, "A design of compact wideband negative group delay network using cross coupling," *Microw. Optical Technology Letters*, Vol. 56, No. 11, 2612–2616, Nov. 2014.
24. Chaudhary, G., Y. Jeong, and J. Lim, "Microstrip line negative group delay filters for microwave circuits," *IEEE Trans. Microw. Theory Tech.*, Vol. 62, No. 2, 234–243, Feb. 2014.
25. Michael, C. T. and T. Itoh, "Maximally flat negative group delay circuit: A microwave transversal filter approach," *IEEE Trans. Microw. Theory Tech.*, Vol. 62, No. 6, 1330–1342, Jun. 2014.
26. Naglich, E. J., J. Lee, D. Peroulis, and W. J. Chappell, "Switchless tunable bandstop to all-pass reconfigurable filter," *IEEE Trans. Microw. Theory Tech.*, Vol. 60, No. 5, 1258–1265, May 2012.
27. Lee, J., E. J. Naglich, H. H. Sigmarsson, D. Peroulis, and W. J. Chappell, "New bandstop filter circuit topology and its application to design of a bandstop to bandpass switchable filter," *IEEE Trans. Microw. Theory Tech.*, Vol. 61, No. 3, 1114–1123, Mar. 2013.
28. Hong, J. S. and M. J. Lancaster, *Microwave Filters for RF/Microwave Applications*, John Wiley & Sons Inc., New York, 2001.